Tricuspid leaflet kinematics after annular size reduction in ovine functional tricuspid regurgitation

Marcin Malinowski, MD, PhD,[a,b] Tomasz Jazwiec, MD,[a,c] Haley Ferguson, BS,[a] Jared Bush, BS,[a] Manuel K. Rausch, PhD,[d] and Tomasz A. Timek, MD, PhD[a]

ABSTRACT

Objective: Tricuspid annular size reduction with annuloplasty rings represents the foundation of surgical repair of functional tricuspid regurgitation. However, the precise effect of annular size reduction on leaflet motion and geometry remains unknown.

Methods: Ten sheep underwent surgical implantation of a pacemaker with an epicardial lead and were paced 200-240 beats/min to achieve biventricular dysfunction and functional tricuspid regurgitation. Subsequently, sonomicrometry crystals were implanted on the right ventricle, the tricuspid annulus, and on the belly of anterior, posterior, and septal tricuspid leaflets. Double-layer polypropylene suture was placed around the tricuspid annulus and externalized to a tourniquet. Simultaneous echocardiographic, hemodynamic, and sonomicrometry data were acquired with functional tricuspid regurgitation and during 5 consecutive annular reduction steps. Annular area, tenting height, and volume, together with each leaflet strain, radial length, and angles, were calculated from crystal coordinates.

Results: Rapid pacing reduced both left ventricle and right ventricle function and induced functional tricuspid regurgitation (0-3+) in all animals (from 0 ± 0 to 2.4 ± 0.7, $P = .002$), whereas tricuspid annulus diameter increased from 2.6 ± 0.3 cm to 3.3 ± 0.3 cm ($P = .001$). Tricuspid annular size reduction 1 to 5 resulted in 16% ± 7%, 37% ± 11%, 55% ± 11%, 66% ± 10%, and 76% ± 8% tricuspid annulus area reduction, respectively, and successively decreased tricuspid regurgitation. Tricuspid annular size reduction 2 to 5 induced anterior and posterior leaflet restricted motion and lower diastolic motion velocities. Tricuspid annular size reduction 5 perturbed septal leaflet range of motion but preserved its angle velocities. Tricuspid annular size reduction 3-5 generated compressive strains in all leaflets.

Conclusions: Tricuspid annular area reduction of 55% perturbed anterior and posterior leaflet motion while maintaining normal septal leaflet movement. More extreme reduction triggered profound changes in anterior and posterior leaflet motion, suggesting that aggressive undersizing impairs leaflet kinematics. (J Thorac Cardiovasc Surg 2021;■:1-12)

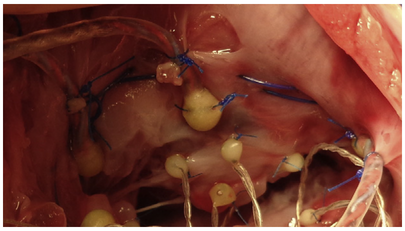

Experimental set-up with crystals implanted on the TV.

CENTRAL MESSAGE

Aggressive TAR perturbs anterior and PL dynamics and geometry in a chronic ovine model of FTR.

PERSPECTIVE

Annular reduction represents the contemporary approach to surgical correction of FTR, but it is unknown how various degrees of annular undersizing influence tricuspid leaflet kinematics. Our experimental data suggest that moderate annular size reduction, although effective at diminishing FTR, least perturbs leaflet geometry, whereas more aggressive annular undersizing severely affects leaflet kinematics.

See Commentary on page XXX.

BS

Tricuspid regurgitation (TR) is a significant predictor of patient mortality and morbidity,[1] with current clinical guidelines advocating a more aggressive surgical approach for repair of less than severe functional tricuspid regurgitation (FTR) associated with a dilated annulus.[2] Tricuspid annuloplasty with prosthetic rings currently represents the surgical gold standard for repair of FTR. Optimal prosthesis sizing still remains a topic of controversy,[3] but a standardized

From the [a]Division of Cardiothoracic Surgery, Spectrum Health, Grand Rapids, Mich; [b]Department of Cardiac Surgery, Medical University of Silesia School of Medicine in Katowice, Katowice, Poland; [c]Department of Cardiac, Vascular, and Endovascular Surgery and Transplantology, Medical University of Silesia School of Medicine in Katowice, Silesian Centre for Heart Diseases, Zabrze, Poland; and [d]Departments of Aerospace Engineering and Engineering Mechanics and Biomedical Engineering, Oden Institute for Computational Engineering and Sciences, University of Texas at Austin, Austin, Tex.

Funding: Meijer Heart and Vascular Institute Internal Grant.

Accepted for the 100th Annual Meeting of The American Association for Thoracic Surgery.

Received for publication June 1, 2020; revisions received Jan 24, 2021; accepted for publication Jan 25, 2021.

Address for reprints: Tomasz A. Timek, MD, PhD, Meijer Heart and Vascular Institute at Spectrum Health, 100 Michigan Ave SE, Grand Rapids, MI 49503 (E-mail: Tomasz.Timek@spectrumhealth.org).

0022-5223/$36.00

https://doi.org/10.1016/j.jtcvs.2021.01.104

Abbreviations and Acronyms

AL = anterior leaflet
ANOVA = analysis of variance
A-P = anteroposterior
CPB = cardiopulmonary bypass
ED = end-diastole
ES = end-systole
IV = intravenously
MR = mitral regurgitation
PL = posterior leaflet
RV = right ventricle
SL = septal leaflet
S-L = septolateral
TAR = tricuspid annular size reduction
TR = tricuspid regurgitation
TV = tricuspid valve

Scanning this QR code will take you to the table of contents to access supplementary information.

approach using undersized rings has been shown to effectively provide durable clinical results.[4,5] The data from studies on the mitral valve have demonstrated that valvular undersizing not only changes annular geometry but also alters physiologic leaflet kinematics.[6] Likewise, implantation of any tricuspid ring invariably changes the geometry, contraction, and strain pattern of the normal tricuspid annulus.[7] We have recently demonstrated that aggressive annular reduction decreases right ventricular (RV) function and attenuates the magnitude of RV strain in both healthy sheep[8] and animals with FTR,[9] yet little is known how annular size reduction affects tricuspid leaflet kinematics and strain. Filling this knowledge gap may aid the design of more physiologic reparative procedures to minimize leaflet stress and promote long-term repair durability. To this end, we set out to investigate the effect of various degrees of tricuspid annular size reduction (TAR) on leaflet geometry, motion, and strain in ovine hearts with chronic FTR.

MATERIALS AND METHODS

All animals received humane care in compliance with the Principles of Laboratory Animal Care formulated by the National Society for Medical Research and the Guide for Care and Use of Laboratory Animals prepared by the National Academy of Science and published by the National Institutes of Health. The study protocol was approved by our local Institutional Animal Care and Use Committee.

Surgical Preparation

Pacemaker implantation. Twenty adult Dorset male sheep were used in the study with the surgical protocol previously described in detail.[9,10] In brief, animals had an external right jugular intravenous catheter placed under local anesthesia with 1% lidocaine injected subcutaneously. Animals were then anesthetized with propofol (2-5 mg/kg intravenously [IV]), intubated, and mechanically ventilated. General anesthesia was maintained with inhalational isoflurane (1%-2.5%). Fentanyl (5-20 μg/kg/min) was infused as additional maintenance anesthesia. A 4F vascular access sheath was introduced through the left carotid artery for arterial blood pressure measurements. Through a left lateral minithoracotomy (fifth/sixth intercostal space), a monopolar pacing lead was sutured onto the lateral LV wall. The lead was exteriorized to a pacemaker (Medtronic Consulta CRT-P, Minneapolis, Minn) placed in the subcutaneous pocket near the spine.

Pacing protocol. After a 5- to 7-day recovery, animals were paced at 200-240 beats/min for 16 ± 4 days to achieve left ventricular ejection fraction less than 30% and at least moderate FTR. Both were monitored with transthoracic echocardiography every 3 days throughout the pacing protocol. When the desired end point was achieved, the animals were taken back to the operating room for the terminal study.

Terminal study. After sedation (ketamine 2-3 mg/kg IV and fentanyl 100 μg IV) and additional local anesthesia (1% lidocaine subcutaneously), a tracheotomy was performed and the animal was intubated and mechanically ventilated. General anesthesia was maintained using isoflurane (1%-2.5%) and fentanyl (5-20 μg/kg/min) with muscle paralysis achieved using vecuronium (0.1 mg/kg IV).

Animals were fully heparinized, and the right carotid artery and right internal jugular vein were exposed in preparation for cardiopulmonary bypass (CPB). The operative procedure was performed through a sternotomy, and the heart was exposed in a pericardial cradle. Caval snares were placed, and the superior and inferior vena cava cannulated with a multistage venous cannula via the right jugular vein. While on CPB and with the heart beating, both cava were snared and the right atrium was opened. Six (2-mm) sonomicrometry crystals (Sonometrics Corp, London, Ontario, Canada) were implanted around the tricuspid annulus, and 12 (1 mm) were sutured on the anterior (4), posterior (4), and septal (4) leaflets in a diamond shape as presented in Figure 1. Sonomicrometry crystal wires were exteriorized through the right atriotomy. Additionally, 13 crystals were implanted on the RV epicardium along the 3 equatorials of RV free wall with additional crystal at the RV apex. Two layers of 2-0 polypropylene sutures were placed around the tricuspid annulus anchored at the anteroseptal commissure and mid-septal annulus. The sutures, representing a modified DeVega-like annuloplasty, were externalized through the anteroposterior (A-P) annulus to a tourniquet allowing for subsequent stepwise suture cinching (Figure 1). The animal was weaned from CPB with epinephrine and milrinone. Pressure transducers (PA4.5-X6; Konigsberg Instruments, Inc, Pasadena, Calif) were placed in the right and left ventricles through the right and left apexes, respectively, and in the right atrium. An electrocardiogram electrode connected to the sonomicrometry system was sutured to the RV free wall. Animals were allowed to stabilize for 30 minutes to achieve steady-state hemodynamics after weaning from CPB. Every animal received lidocaine IV drip (0.03 mg/kg/min) to prevent ventricular ectopy. All animals were studied under open-chest experimental conditions.

Data acquisition. Progressive tricuspid annular area reduction (TAR) simulating reductive annuloplasty was achieved by 5 consecutive (8-10 mm) pulls of the annular suture against the hemostat. Simultaneous hemodynamic, echocardiographic, and sonomicrometry data were acquired before suture cinching (FTR) and with each consecutive tricuspid annular reduction (TAR1-5).

All sonomicrometry data were acquired using a Sonometrics Digital Ultrasonic Measurement System DS3 (Sonometrics Corp) as previously

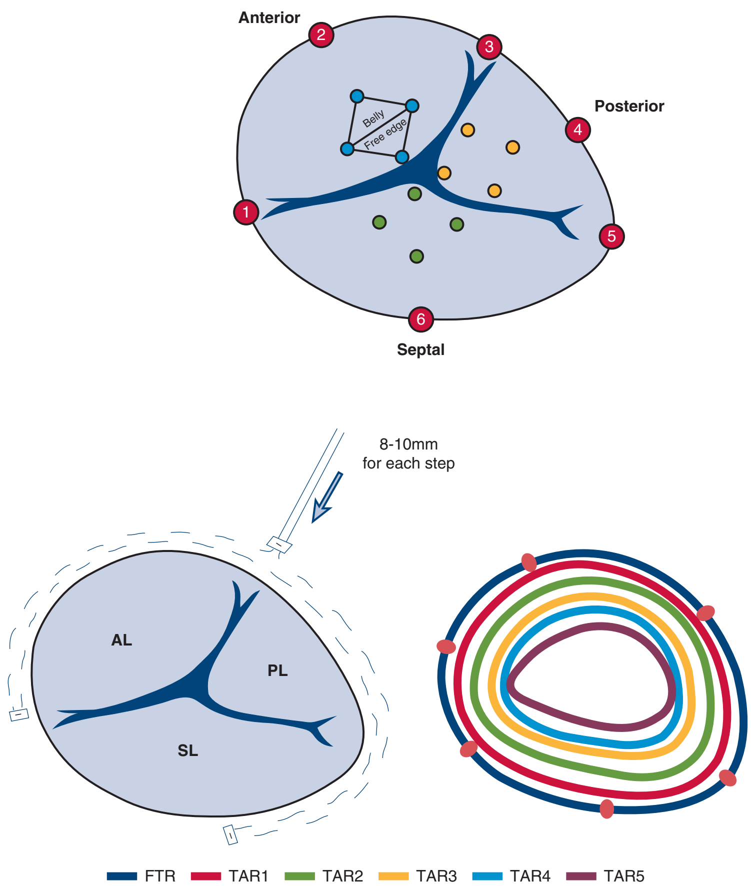

FIGURE 1. Schematic representation of the experimental setup showing the location of the sonomicrometry crystals implanted on the tricuspid annulus and valve leaflets (*top*) and tricuspid annular reduction used with its effect on the annular shape (*bottom*). Two layers of DeVega-like 2-0 polypropylene suture were placed around the tricuspid annulus and cinched gradually at every TAR step of 8-10 mm. The annular models were obtained from least-squares cubic spline fit to the position of annular crystals at each step. *AL*, Anterior leaflet; *FTR*, functional tricuspid regurgitation; *PL*, posterior leaflet; *SL*, septal leaflet; *TAR*, tricuspid annular reduction.

described.[11] Data from 3 consecutive heart cycles acquired at 128 Hz during sinus rhythm and steady-state hemodynamic conditions were merged to yield 3-dimensional coordinates of each sonomicrometry crystal for baseline condition (FTR) and each step of tricuspid annular reduction (TAR1-5). The time-resolved 3-dimensional crystal coordinates obtained from the SonoSoft software (Sonometrics Corp.) were analyzed in MATLAB (MathWorks, Natick, Mass) using custom-written code.

All values were calculated at end-systole (ES) and end-diastole (ED). ED was defined as the time of the beginning of positive deflection in electrocardiogram voltage (R wave), and ES was determined as the time of maximum negative dp/dt of left ventricular pressure.

Epicardial echocardiography to evaluate biventricular function, valvular insufficiency, and tricuspid transvalvular gradient was performed during the terminal surgery. All images were acquired with Vivid S6 (GE Healthcare, Chicago, Ill) using a 1.5- to 3.6-Mhz probe. The degree of valvular insufficiency was assessed using American Society of Echocardiography criteria. The grading included comprehensive evaluation of color flow and continuous-wave Doppler. Tricuspid and mitral regurgitation (MR) were graded accordingly and categorized by an experienced cardiologist as none or trace (0), mild (+1), moderate (+2), or severe (+3).

At the conclusion of the experiment, the animals were euthanized by administering sodium pentothal (100 mg/kg IV) and potassium chloride bolus (80 mEq IV). The heart was excised, and the proper placement of crystals was confirmed.

Data Analysis

Tricuspid valve geometry and dynamics.

Tricuspid annular area and perimeter were calculated on the basis of the spline fit of annular crystals as previously described.[12,13] Septolateral (S-L) annular dimension was calculated as the distance between crystals 2 and 6; A-P annular dimension was calculated as the distance between crystals 1 and 4 (Figure 1). Annular contraction was calculated as the percent difference between maximal and minimal annular area ($[A_{max} - A_{min}]/A_{min} \times 100\%$).[7,12] Regional annular contraction was defined as the percentage difference between maximal and minimal regional perimeter.[7] RV volume was calculated using convex hull method based on annular and ventricular crystal coordinates.[8] Tenting volume was calculated using convex hull method as the volume enclosed by all annular and leaflet crystals. Tenting height was measured for each leaflet as the perpendicular distance between the tip of leaflet and the tricuspid annular plane. Tricuspid valve (TV) tenting height was measured as the perpendicular distance from annular plane to the centroid of all 3 leaflet tip crystals.

Leaflet kinematics.

Tricuspid leaflet lengths were computed on the basis of radial spline fit of the mid-regional annular crystal, mid-belly

TABLE 1. Hemodynamics after tricuspid annular size reduction

(n = 10)	FTR	FTR + TAR1	FTR + TAR2	FTR + TAR3	FTR + TAR4	FTR + TAR5	*P*
HR (bpm)	130 ± 15	129 ± 19	130 ± 20	128 ± 21	127 ± 22	120 ± 33	.350
LVP_{max} (mm Hg)	101 ± 15	96 ± 21	94 ± 22	85 ± 22	80 ± 23	75 ± 23*	.001
LVP_{ES} (mm Hg)	68 ± 12	64 ± 17	63 ± 15	57 ± 15	54 ± 11*	49 ± 12*	<.001
LVP_{ED} (mm Hg)	13 ± 3	13 ± 3	13 ± 3	12 ± 3	12 ± 4	12 ± 4	.204
RVP_{max} (mm Hg)	51 ± 13	49 ± 12	48 ± 13	46 ± 13	43 ± 11	41 ± 12	.006
RVP_{ES} (mm Hg)	42 ± 13	40 ± 11	39 ± 10	37 ± 10	35 ± 11	32 ± 10*	.007
RVP_{ED} (mm Hg)	14 ± 8	14 ± 7	14 ± 7	15 ± 8	15 ± 9	15 ± 8	.279
RAP (mm Hg)	6 ± 3	6 ± 3	7 ± 3	8 ± 3	9 ± 3	10 ± 3*	.006
RV EDV (mL)	160 ± 24	156 ± 24	155 ± 26	146 ± 22*	142 ± 27*	137 ± 31*	<.001
RV FVC (%)	19 ± 5	17 ± 7	15 ± 8	13 ± 7*	11 ± 7*	8 ± 5*	<.001
Mean TV gradient (mm Hg)	0.7 ± 0.3	0.9 ± 0.3	1.2 ± 0.4	2.3 ± 1.1	2.9 ± 1.8*	3.6 ± 1.4*	.002

Data shown as mean ± standard deviation. *P* value from repeated-measures ANOVA. *FTR*, Functional tricuspid regurgitation; *TAR*, tricuspid annular reduction; *HR*, heart rate; *LVP*, left ventricular pressure; *ES*, end systole; *ED*, end-diastole; *RVP*, right ventricular pressure; *RAP*, right atrial pressure; *RV*, right ventricle; *EDV*, end-diastolic volume; *FVC*, fractional volume change; *TV*, tricuspid valve. **P* < .05 versus FTR with paired *t* test.

BS

crystal, and free edge crystal. Anterior, posterior, and septal leaflet (SL) angles were calculated as an angle between the annular plane and a vector leading from the corresponding mid-annular crystal to the free edge crystal. Leaflet excursion angle was calculated as a difference between maximal opening and minimal closing angles. Angle velocities were calculated during diastole and systole to assess valve opening and closing conditions.[14]

Leaflet strains. *Cardiac strains.* Leaflet strains in the beating heart were calculated on the basis of leaflet crystal coordinates using the approach previously described.[15] In brief, 8 triangles were used to discretize every leaflet based on annular and leaflet crystals. Each triangular element was interpolated via linear shape functions to characterize surface deformation. Leaflet "belly" and "free edge" regions (triangles) were defined by 1-mm leaflet crystals (Figure 1). Green-Lagrange area strains were calculated for each leaflet. Areal strains combine changes in circumferential and longitudinal directions and thus represent the directionally independent total deformation. Average cardiac cycle strains, a measure of leaflet regional deformation, were calculated for each leaflet belly and free edge with ED as the reference state.

Interventional strains. Interventional strains, assessing the direct effect of annular size reduction on each of 3 tricuspid leaflets, were calculated at ES for all interventions (TAR1-5) with the same time point at FTR serving as the reference. Negative or "compressive" strains imply that tissue is compressed, whereas positive strains imply that tissue is stretched.

Statistical Analysis

Data are presented as mean ± 1 standard deviation or median with 25th and 75th percentiles when normality assumptions (Shapiro–Wilk test) were not met. The measured variables were compared with

TABLE 2. Tricuspid valve geometry and dynamics after tricuspid annular size reduction

(n = 10)	FTR	FTR + TAR1	FTR + TAR2	FTR + TAR3	FTR + TAR4	FTR + TAR5	*P*
Annular reduction (%)	0	16 ± 7*	37 ± 11*	55 ± 11*	66 ± 10*	76 ± 8*	<.001
TR grade	2.5 (2.0-3.0)	2.0 (0.375-2.75)	2.0 (0.375-2.0)	1.25 (0.25-2.0)†	0.5 (0-1.5)†	0 (0:1.38)†	<.001
Area (mm^2)							
Maximal	869 ± 143	738 ± 155†	557 ± 159†	398 ± 155†	303 ± 109†	207 ± 79†	<.001
Minimal	811 ± 131	695 ± 143†	533 ± 153†	381 ± 134†	288 ± 107†	199 ± 78†	<.001
Annular contraction (%)							
Global	6.9 (4.7-8.0)	5.2 (3.8-6.9)	3.4 (3.1-6.0)	3.5 (1.8-5.8)†	4.1 (1.8-7.3)	3.3 (1.8-5.7)	.021
Anterior	7 ± 1	5 ± 2	5 ± 1	6 ± 2	5 ± 2	5 ± 2	.055
Posterior	4 ± 1	3 ± 1	4 ± 1	4 ± 2	4 ± 1	4 ± 2	.477
Septal	6 ± 2	6 ± 2	6 ± 3	6 ± 2	6 ± 2	5 ± 3	.684
Perimeter (mm)							
Maximal	107 ± 8	99 ± 9†	87 ± 11	75 ± 10†	66 ± 9†	57 ± 7†	<.001
Minimal	104 ± 8	97 ± 9†	85 ± 11†	73 ± 10†	65 ± 9†	56 ± 8†	<.001
S-L $diameter_{ED}$ (mm)	31.0 ± 3.6	28.3 ± 3.7†	25.4 ± 4.4†	21.8 ± 4.0*	19.6 ± 3.3†	16.8 ± 3.5†	<.001
A-P $diameter_{ED}$ (mm)	30.4 ± 3.7	27.3 ± 3.8†	22.5 ± 3.7†	18.9 ± 3.9†	16.3 ± 3.6†	13.6 ± 3.3†	<.001
TV tenting $volume_{ES}$ (mL)	3.2 (2.8-4.0)	3.0 (2.3-3.9)	2.4 (1.9-3.4)†	2.1 (1.5-2.6)†	1.9 (1.2-2.1)†	1.3 (1.0-1.8)†	<.001
TV tenting $height_{ES}$ (mm)	9.8 ± 1.3	10.1 ± 1.4	10.4 ± 1.6	10.8 ± 1.9	11.0 ± 2.2	11.1 ± 2.6	.050

Data shown as mean ± standard deviation or median with 25th and 75th percentile when normality assumptions (Shapiro–Wilk test) were not met. *P* values from repeated-measures ANOVA/Friedman ANOVA. *FTR*, Functional tricuspid regurgitation; *TAR*, tricuspid annular reduction; *S-L*, septolateral; *ED*, end-diastole; *A-P*, anteroposterior; *TV*, tricuspid valve; *ES*, end systole. **P* < .05 with Bonferroni test versus the preceding TAR level. †*P* < .05 versus FTR with paired *t* test or Wilcoxon test.

within-subject repeated-measures analysis of variance (ANOVA) or Friedman repeated-measures ANOVA. The latter was used if any time-point data were deemed non-normally distributed. Greenhouse-Geisser correction was applied to sphericity assumption. Whenever ANOVA yielded significance (P < .05), then each intervention (TAR1-5) was compared with FTR with the paired t test. After significant Friedman's ANOVA, Wilcoxon matched-pairs signed rank test was used for multiple comparisons versus FTR. Bonferroni correction was used to adjust the P value to account for multiple comparisons. Size of annular reduction in TAR1-5 was assessed with repeated-measures ANOVA followed by Bonferroni multiple comparison test to evaluate each TAR level with the preceding state. GraphPad Prism 8.4.3 (GraphPad Software, San Diego, Calif) was used for all statistical analysis.

RESULTS

Ten sheep (62 ± 6 kg) completed the pacing protocol and terminal procedure with successful acquisition of sonomicrometry, hemodynamic, and echocardiographic data. Two animals died during the pacing period. Eight sheep were excluded for the following reasons: pacemaker failure (1), sonomicrometry crystals failure (2), and inability to wean from the CPB (5).

Hemodynamics

Hemodynamic characteristics are shown in Table 1. There was no difference in heart rate but RV fractional volume change progressively declined with TAR3-5. Progressive TAR resulted in increased mean pressure gradient across the TV, although well below a clinical level for the diagnosis of significant tricuspid stenosis. TAR4 and 5 were associated with decreased LV pressure, and TAR5 increased right atrial pressure and caused a decrease in RV systolic pressure compared with FTR.

Tricuspid Regurgitation, Annular Geometry, and Annular Dynamics

After pacing, TR (0-3+) increased from 0 to 2.5 (2.0-3.0) (P = .002). Each step of TAR gradually decreased TR grade to 2.0 (0.375-2.75), 2.0 (0.375-2.0), 1.25 (0.25-2.0), 0.5 (0-1.5), and 0 (0-1.38) for TAR1-5, respectively. Only TAR3-5 significantly reduced tricuspid insufficiency relative to FTR (Table 2).

Tricuspid annular geometry and dynamics with FTR and each step of TAR are presented in Table 2. The stepwise annular cinching resulted in gradual, significant at every step, decrease in tricuspid annular size with TAR1-5 resulting in 16%, 37%, 55%, 66%, and 75% annular area reduction, respectively. A significant decrease in annular perimeter was also observed. We observed significant reduction in annular size in both S-L and A-P directions, but regional annular perimeter contraction remained unaltered. TAR2-5 was associated with a significant decrease

TABLE 3. Leaflet geometry and dynamics during tricuspid annular reduction

(n = 10)	FTR	FTR + TAR1	FTR + TAR2	FTR + TAR3	FTR+TAR4	FTR+TAR5	P
AL							
Leaflet length$_{ES}$ (mm)	22.5 ± 2.8	21.2 ± 2.8	20.4 ± 3.5*	19.1 ± 3.7*	18.1 ± 4.1*	17.7 ± 4.4*	.001
Tenting height (mm)	7.4 (6.4-9.2)	7.1 (5.7-9.7)	8.1 (7.3-10.3)*	10.0 (7.7-11.6)*	10.1 (8.2-13.0)*	9.8 (7.6-12.8)*	<.001
Opening angle$_{max}$ (°)	64 ± 10	63 ± 10	63 ± 11	65 ± 13	62 ± 11	60 ± 17	.617
Closing angle$_{min}$ (°)	25 (17-28)	24 (21-29)	29 (26-33)*	36 (30-41)*	43 (39-48)*	45 (31-58)*	<.001
Excursion angle (°)	38 ± 13	35 ± 11	30 ± 11*	25 ± 12*	17 ± 10*	13 ± 8*	<.001
Opening velocity (°/ms)	0.68 ± 0.20	0.67 ± 0.19	0.65 ± 0.14	0.49 ± 0.23*	0.37 ± 0.20*	0.28 ± 0.18*	<.001
Closing velocity (°/ms)	0.69 ± 0.32	0.67 ± 0.24	0.57 ± 0.22	0.50 ± 0.22	0.30 ± 0.13*	0.28 ± 0.17*	<.001
PL							
Leaflet length$_{ES}$ (mm)	15.9 (14.0-17.3)	15.8 (14.0-17.4)	15.1 (13.4-17.0)	14.5 (13.4-17.0)	15.4 (13.5-17.3)	15.1 (12.6-16.8)	.259
Tenting height (mm)	8.5 ± 2.8	9.4 ± 2.4	10.0 ± 2.0	11.1 ± 1.9*	11.6 ± 2.0*	11.3 ± 2.2*	<.001
Opening angle$_{max}$ (°)	73 ± 8	74 ± 8	74 ± 7	77 ± 7	77 ± 8	74 ± 9	.443
Closing angle$_{min}$ (°)	39 ± 15	43 ± 11*	49 ± 8*	56 ± 7*	60 ± 6*	61 ± 7*	<.001
Excursion angle (°)	34 ± 15	31 ± 13	25 ± 9*	21 ± 8*	16 ± 8*	13 ± 7*	<.001
Opening velocity (°/ms)	0.72 ± 0.24	0.68 ± 0.30	0.54 ± 0.27	0.48 ± 0.31	0.36 ± 0.17*	0.27 ± 0.11*	<.001
Closing velocity (°/ms)	0.59 (0.46-0.77)	0.50 (0.42-0.85)	0.42 (0.34-0.73)	0.38 (0.28-0.61)*	0.37 (0.25-0.50)*	0.25 (0.19-0.50)*	.002
SL							
Leaflet length$_{ES}$ (mm)	14.6 ± 3.8	14.1 ± 4.0	13.6 ± 3.9	13.3 ± 3.9	13.7 ± 3.7	12.9 ± 3.3	.114
Tenting height (mm)	7.0 ± 2.4	7.2 ± 2.6	7.5 ± 2.6	7.8 ± 2.4	8.1 ± 2.2	8.3 ± 2.4	.053
Opening angle$_{max}$ (°)	55 ± 13	59 ± 12*	61 ± 14*	65 ± 16*	64 ± 16*	62 ± 13*	<.001
Closing angle$_{min}$ (°)	25 ± 9	26 ± 8	32 ± 9*	36 ± 11*	39 ± 10*	42 ± 9*	<.001
Excursion angle (°)	30 ± 10	32 ± 11	30 ± 12	28 ± 14	24 ± 13	20 ± 12*	<.001
Opening velocity (°/ms)	0.53 ± 0.22	0.57 ± 0.26	0.53 ± 0.28	0.50 ± 0.19	0.47 ± 0.35	0.43 ± 0.30	.370
Closing velocity (°/ms)	0.49 (0.41-0.62)	0.60 (0.42-0.77)	0.53 (0.38-0.75)	0.55 (0.32-0.84)	0.44 (0.23-0.77)	0.35 (0.17-0.57)	.052

Data shown as mean ± standard deviation or median with interquartile range (25th-75th percentiles). P values from repeated-measures ANOVA/Friedman ANOVA. *FTR*, Functional tricuspid regurgitation; *TAR*, tricuspid annular reduction; *AL*, anterior leaflet; *ES*, end systole; *PL*, posterior leaflet; *SL*, septal leaflet. *P < .05 versus FTR with paired t test or Wilcoxon test. Leaflet length was calculated as the sum of end-systolic distances between the midline leaflet crystals and mid annular crystal (Figure 2).

in tenting volume compared with FTR, whereas TV tenting height did not change.

Leaflet Geometry and Dynamics

The successive steps of tricuspid annular reduction resulted in progressive decrease of anterior leaflet (AL) radial length (TAR2-5) with no effect on posterior or SL length (Table 3). Tenting height increased with TAR2-5 for AL and TAR3-5 for PL, but there was no change in tenting height of SL during the entire protocol. Opening angle of the anterior and posterior leaflets (PLs) remained unaltered by all steps of TAR, but SL opening angle increased starting early with TAR1. TAR3-5 increased closing angle of all 3 leaflets (Figure 2). The excursion angle, representing the range of leaflet motion, was diminished after TAR2-5 in AL and PL and only after TAR5 in SL (Figure E1). The dynamics of leaflet motion represented by opening and closing angular velocities were decreased after aggressive TAR for AL and PL. SL velocities remained unaffected at any TAR level (Table 3). AL,

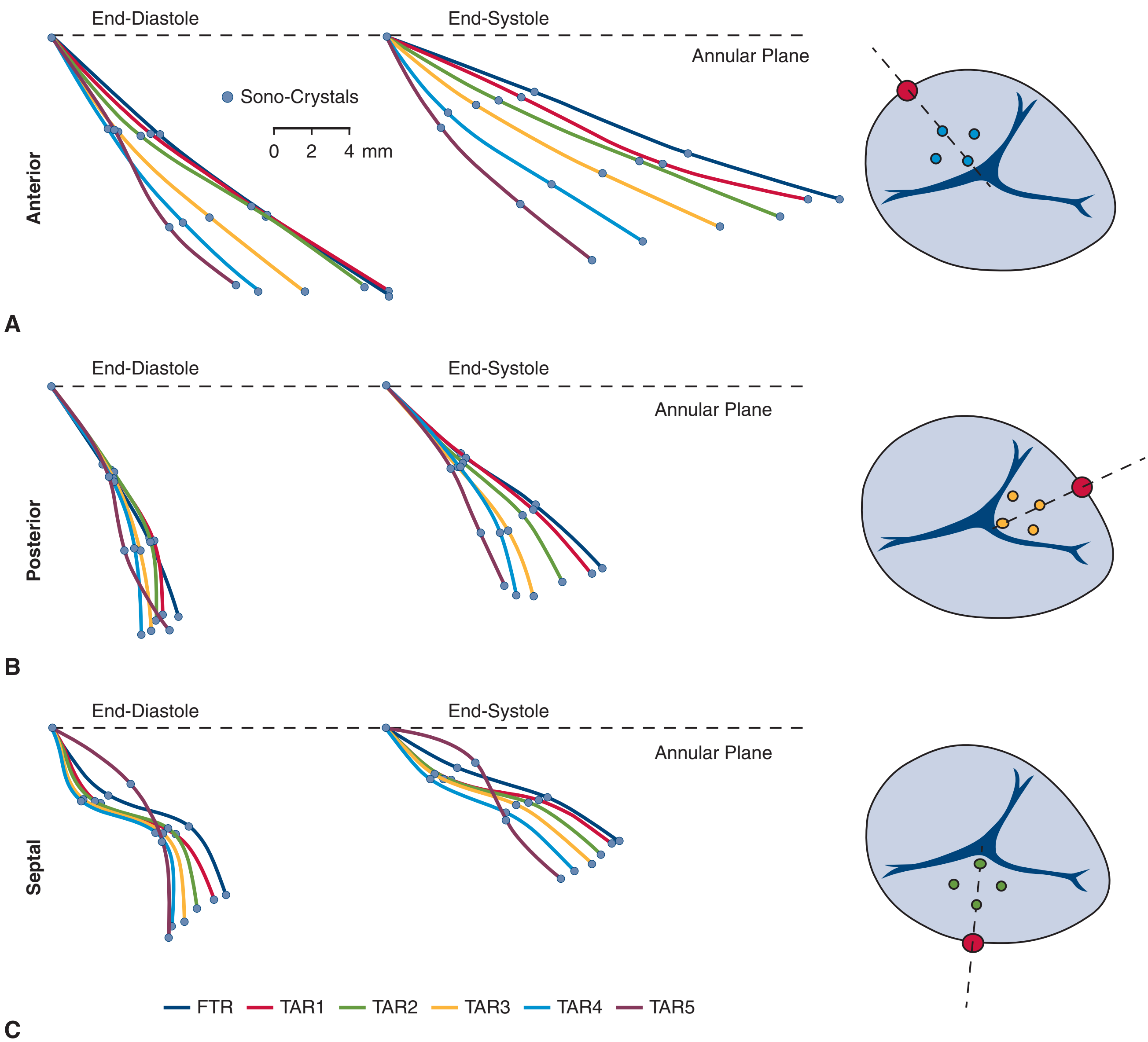

FIGURE 2. Kinematics of the radial cross-section centerline for anterior (A), posterior (B), and septal (C) leaflets with FTR and after TAR1-5 at ED (*left*) and ES (*right*). Opening angle of the anterior and PLs remained unaltered by all steps of TAR, but SL opening angle increased. TAR3-5 increased closing angle of all 3 leaflets. Each radial centerline across the leaflet was computed as the least-squares cubic spline created by connecting appropriate mid annular, mid belly, and the free edge leaflet crystal as well as a fourth crystal position, which we created by calculating the mean position of the 2 lateral crystals. *FTR*, Functional tricuspid regurgitation; *TAR*, tricuspid annular reduction.

PL, and SL movement with each step of TAR during cardiac cycle are shown in Videos 1 to 3.

Leaflet Strains

The effects of annular size reduction on cardiac and interventional leaflet strains for both leaflet belly and free edge are presented in Figures 3 and 4, respectively.

Cardiac strains. The most perturbed regional strain by annular size reduction was the belly of the AL where the magnitude of strain decreased gradually from 49% ± 34% (FTR) to 6% ± 14% with TAR5 ($P = .009$). The free edge strain in the AL remained unaffected. There was no change in strain magnitude in both regions of the PL. TAR3-5 decreased areal strain in the belly of the SL, but only TAR5 affected its free edge (Figure 3).

Interventional strains. TAR3-5 induced compressive strains in both leaflet regions in anterior and PL and the belly region of the SL. There was no direct effect of any TAR on the septal free edge interventional strain (Figure 4).

DISCUSSION

The current study using a chronic ovine model of FTR revealed that TAR of at least 55% was effective in diminishing TR, but this degree of annular size reduction induced nonphysiologic leaflet dynamics. More aggressive annular cinching was accompanied by reduced leaflet range of

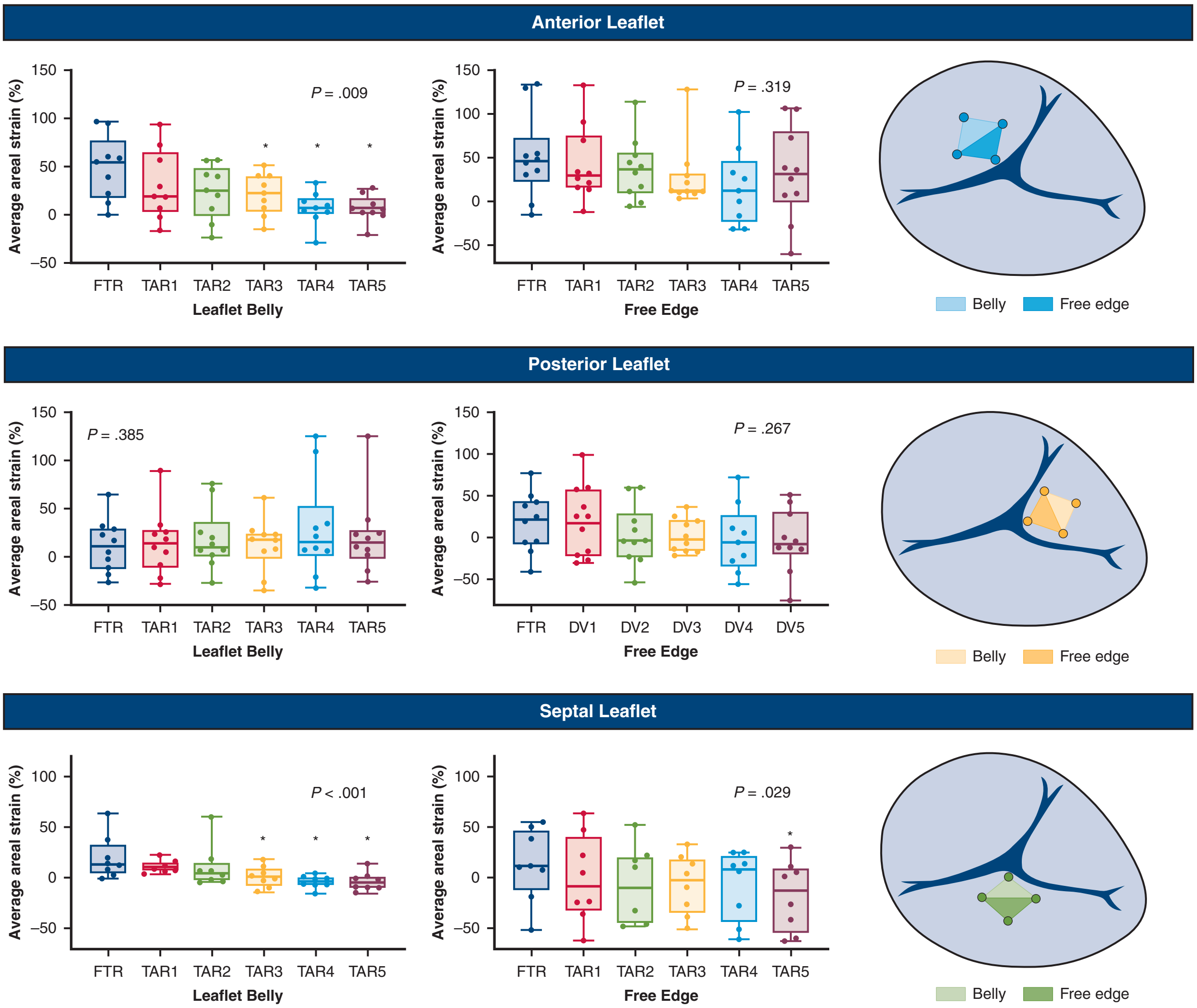

FIGURE 3. Tricuspid leaflet mean systolic areal cardiac strains for each leaflet belly and free edge with FTR and during TAR1-5. Anterior (*top*), posterior (*middle*), and septal (*bottom*) leaflet. Strains are presented at ES for FTR and each intervention (TAR1-5) with the reference configuration at ED. TAR3-5 resulted in the decrease of leaflet belly areal strain in anterior and SL with no effect on the PL. The *upper* and *lower borders* of the box represent the upper and lower quartile. The *middle horizontal line* represents the median. The *upper* and *lower whiskers* represent the maximum and minimum values. *P* values from repeated-measures ANOVA/Friedman ANOVA. *$P < .05$ versus FTR with paired *t* test or Wilcoxon test. *FTR*, Functional tricuspid regurgitation; *TAR*, tricuspid annular reduction.

BS

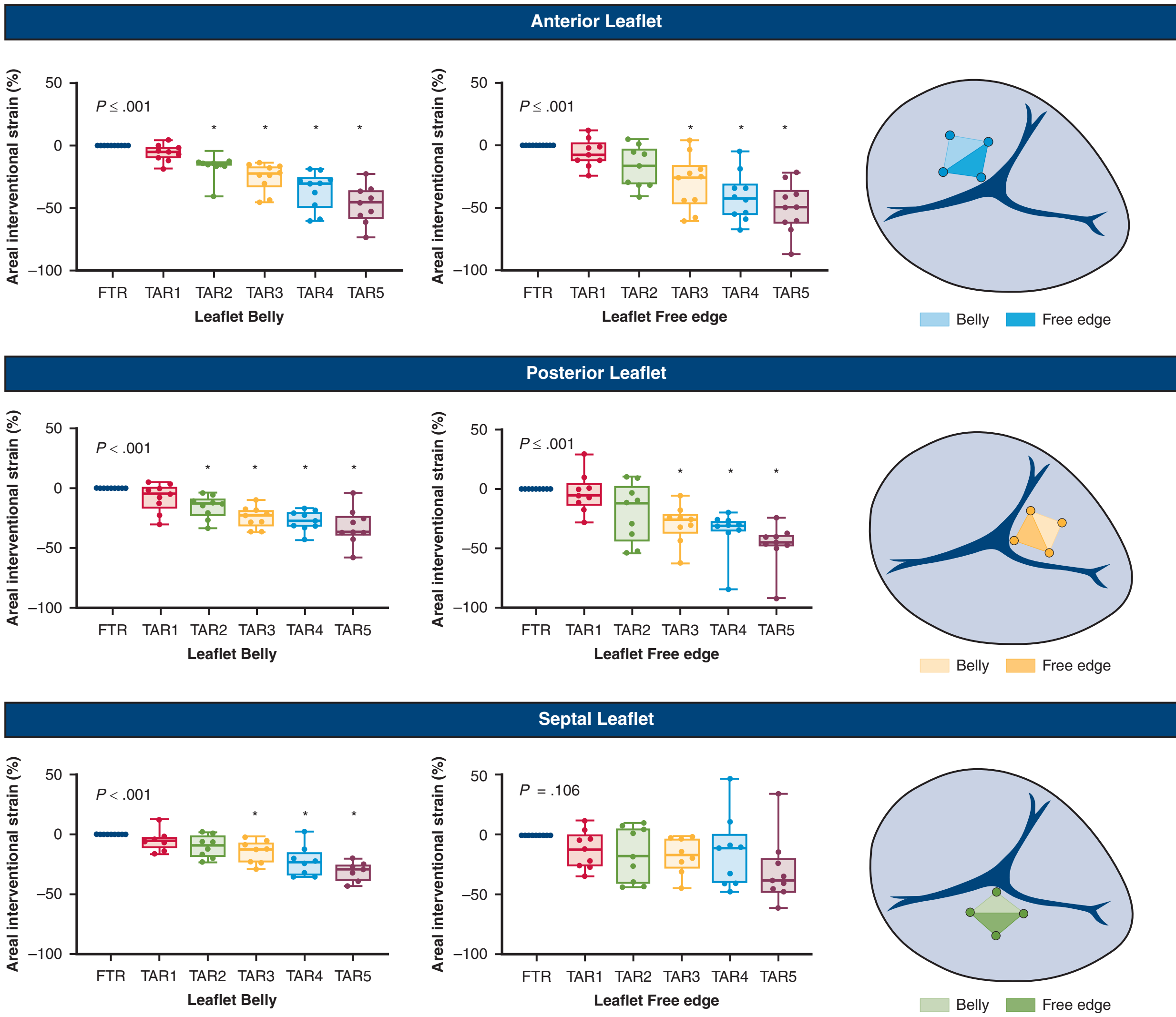

FIGURE 4. Tricuspid leaflet average areal interventional strains with FTR and during TAR1-5 for anterior (*top*), posterior (*middle*), and septal (*bottom*) leaflet. Strains are presented at ES for each intervention (TAR1-5) with the reference configuration at FTR. The positive values indicate leaflet stretch, whereas the negative values indicate leaflet compression. TAR3-5 induced compressive strains in both leaflet regions in anterior and PL and the belly region of the SL. There was no direct effect of any TAR on the septal free edge interventional strain. The *upper* and *lower borders* of the box represent the upper and lower quartiles. The *middle horizontal line* represents the median. The *upper* and *lower whiskers* represent the maximum and minimum values. *P* values from repeated-measures ANOVA/Friedman ANOVA. *$P < .05$ versus FTR with paired *t* test or Wilcoxon test. *FTR*, Functional tricuspid regurgitation; *TAR*, tricuspid annular reduction.

motion, altered closure kinematics, and compressive strain patterns in the leaflet belly (Figure 5). To our best knowledge, this is the first report describing tricuspid leaflet strains and kinematic after surgical repair of FTR.

The concept of annular undersizing during surgical annuloplasty was introduced for the repair of functional MR by Bolling and colleagues[16] as an "annular solution to a ventricular problem." Similar to functional MR, FTR results from pathological changes at both the ventricular and the valvular level. RV dilation and dysfunction leading to tricuspid annular enlargement and leaflet tethering represent the key components of the vicious cycle in the development and perpetuation of FTR.[17] Correspondingly, the concept of undersized annuloplasty has also been adopted for the TV. Despite promising clinical results using this approach,[5,18] there are limited data describing tricuspid leaflet dynamics and geometry after surgical repair. One of the few studies that analyzed leaflet geometry before and after annuloplasty was by Min and colleagues.[19] Comparable to our results, these investigators found that tenting of all 3 leaflets became aggravated after TV repair regardless of the annuloplasty technique used. These observations were associated with increased tenting (closing) angles of all leaflets. Although the authors did not report

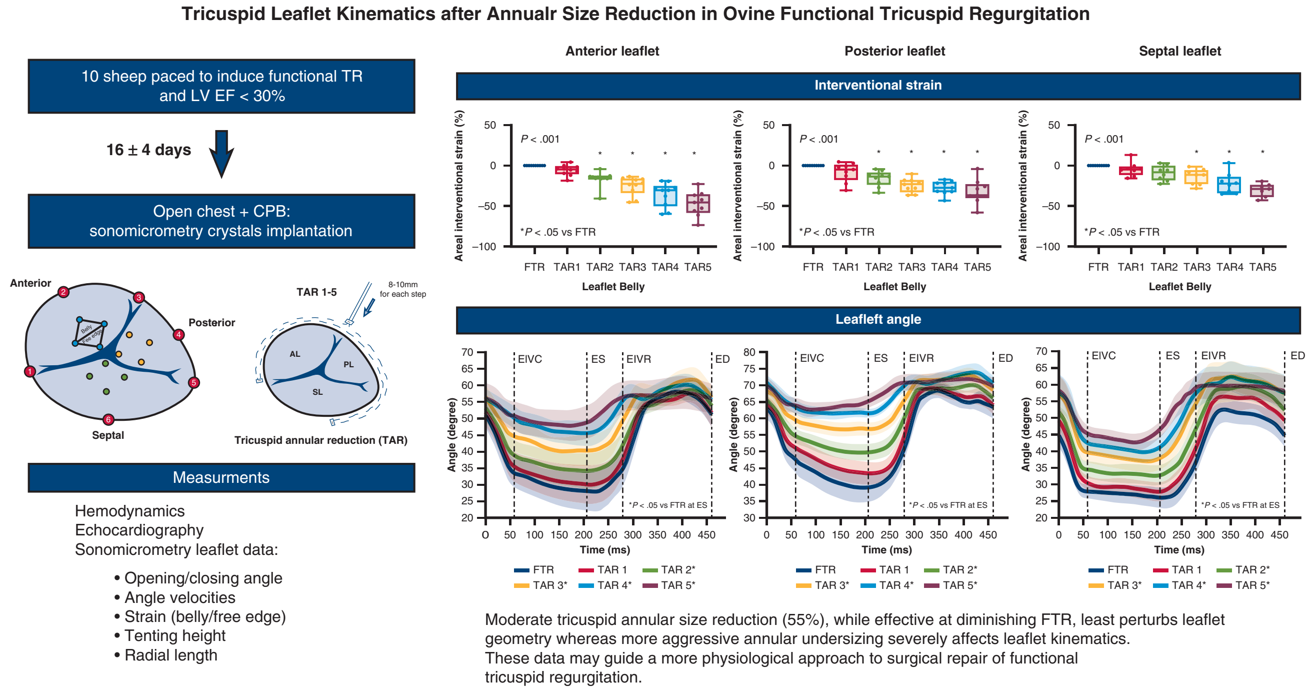

FIGURE 5. Tricuspid leaflet strain and dynamics changes after 5 levels of TAR in ovine model of FTR. The parameters were calculated on the basis of 3-dimensional coordinates of 6 implanted onto the annulus and 12 on 3 tricuspid leaflets sonomicrometry crystals. Moderate annular size reduction (55%), although effective at diminishing FTR, least perturbs leaflet geometry, whereas more aggressive annular undersizing severely affects leaflet kinematics. *FTR*, Functional tricuspid regurgitation; *LV*, left ventricular; *EF*, ejection fraction; *CPB*, cardiopulmonary bypass; *EIVC*, end of isovolumic contraction; *ES*, end-systole; *EIVR*, end of isovolumic relaxation; *ED*, end-diastole; *TAR*, tricuspid annular reduction.

the size of implanted rings, the described 38% decrease of S-L diameter would correspond to TAR4 annular reduction of the current study. Experimental studies on the mitral valve have shown that leaflet mechanics and geometry are highly unphysiologic after both true size[20] and undersized[6] prosthetic annuloplasty and may lead to pathologic changes in leaflet structure.[6] On the other hand, Tibayan and colleagues[21] demonstrated that suture annuloplasty did not perturb mitral leaflet excursion angles in acute ovine ischemic MR, but the annulus was not reduced substantially in that study. The S-L annular dimension was decreased by only 4%, whereas in our study TAR1 decreased S-L annular dimension by 9% ± 4%, TAR3 by 30% ± 8%, and TAR5 by 46% ± 9%. In experimental animals, Bothe and colleagues[20] reported reduction of mitral valve opening regardless of annuloplasty ring type and observed increased closing and opening angle velocities with saddle-shaped rigid rings. However, these investigators studied healthy animals and used true-sized rings.

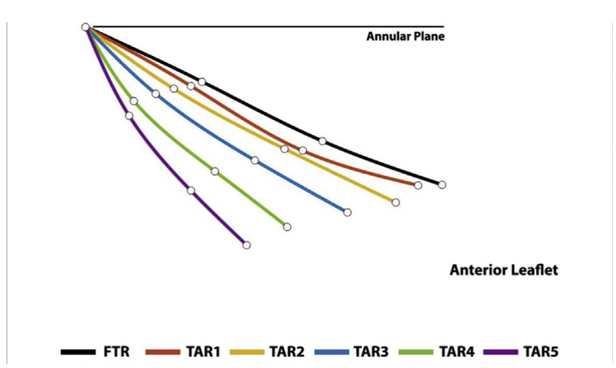

VIDEO 1. Tricuspid AL movement with various levels of annular cinching. Video available at: https://www.jtcvs.org/article/S0022-5223(21)00203-8/fulltext.

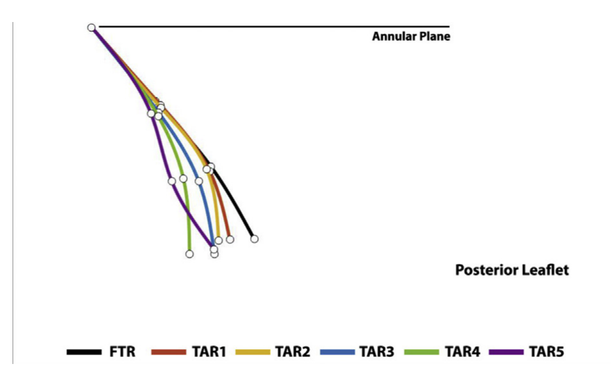

VIDEO 2. Tricuspid PL movement with various levels of annular cinching. Video available at: https://www.jtcvs.org/article/S0022-5223(21)00203-8/fulltext.

BS

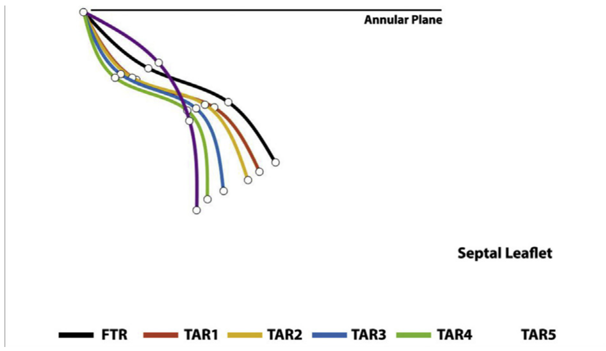

VIDEO 3. Tricuspid SL movement with various levels of annular cinching. Video available at: https://www.jtcvs.org/article/S0022-5223(21)00203-8/fulltext.

The differential dynamics of the 3 tricuspid leaflets in response to annular undersizing may be related to their heterogenous mechanobiological properties. We have recently shown that collagen orientation and valve cell nuclear morphology vary between leaflets with the SL being most stiff,[22] potentially contributing to its maintained physiology with all but the most aggressive undersizing. Moreover, dissimilar changes in leaflet dynamics could be related to different leaflet size and distinct anatomic origin of each of 3 tricuspid leaflets.[23]

BS

The shorter length of the AL measured in the current study after aggressive undersizing suggests folding of the leaflet, and leaflet length was previously found to be an independent predictor of residual TR after annuloplasty.[24] In this context, the "decrease" of available coaptation surface of the AL and the increased tenting height suggest persistent tethering. Furthermore, the inward displacement of the annulus (Figure 1) with concomitant changes in closing angles seen in the AL and PL with undersizing are clearly indicative of subvalvular changes and tethering. Leaflet tethering associated with restrictive mitral annuloplasty has been shown to induce biological changes in leaflets, including increase of collagen synthesis and elevation of transforming growth factor-β.[6] These in turn promote fibrosis, thickening, and calcification and may contribute to suboptimal long-term clinical results.[25] To prevent chronic, postrepair tethering, subvalvular interventions[26] or AL augmentation[27] may be warranted to achieve failure free results.

Although tricuspid leaflet strains have been studied in both computational models[28] and in vivo,[15] there is a dearth of knowledge on how they are influenced by reductive annuloplasty. Altered mitral valve geometry after annuloplasty has been shown to perturb normal leaflet strains[29]; therefore, it is not surprising that perturbations in tricuspid leaflet strains were observed in our study with annular undersizing. Significant alterations in strain were observed only in the leaflet belly of AL and SL with the free edge regions mostly spared. These regional differences may be related to spatial variability of tricuspid leaflet mechanical properties. Laurence and colleagues[30] reported that the central portion of the leaflets exhibit greater material anisotropy than free edge regions. Moreover, extensibility and peak stretch values were found to be lower in the leaflet edge. Differential biomechanical behavior has also been described among the 3 TV leaflets with the greatest extensibility and anisotropy observed in the PL.[31] These observations may partially explain our findings of no alterations in PL cardiac strain with progressive annular reduction. We can speculate that the progressive decrease in strain magnitude observed with TAR3-5 potentially changes leaflet mechanobiological homeostasis and may result in subsequent tissue remodeling, but this hypothesis requires further studies for substantiation.

Mitral annuloplasty has been shown to decrease leaflet stresses as a function of ring size,[32] yet it is unknown whether this holds true for the TV. Because of the known linear strain-stress relation described in the mitral valve,[33] we can extrapolate that the observed decrease in leaflet strain in our study may be related to TAR-induced reduction of leaflet stress. However, the equilibrium between leaflet stress optimization and possible adverse effects from aggressive undersizing needs better characterization. Following the principles for mitral repair, the goal of the surgical repair of FTR should not be limited to achieve a competent valve but also to minimize the tissue stress. However, the extrapolation of mitral valve data to the right side should be done with caution because there is clear evidence that the leaflets of these 2 atrioventricular valves differ substantially in both microstructural and biomechanical properties.[22,34,35] Furthermore, 3-leaflet anatomy and 3 papillary muscles with direct septal insertion make the TV mechanistically different and more complex than its left side counterpart.

Study Limitations

Several study limitations should be considered in the interpretation of the results of the current study. This was an animal study, and clinical extrapolation of the results must be done with extreme caution. Sheep is a large animal model considered to best reflect human cardiac physiology.[36] The anatomy of the cardiac valves closely resembles the human, making the ovine model a reliable one to study valvular pathologies.[37] Sheep cardiovascular physiology is comparable to human with similar heart rate and arterial pressure values. The size of the heart and chest cavity and vascular anatomy also resemble those of the human and are large enough to allow performance of clinically pertinent surgical procedures. Our experiment was performed in open-chest, open pericardium sheep under anesthesia, and we have previously shown that the anesthesia may affect tricuspid annular dynamics but does not alter geometry.[38]

Sonomicrometry crystals by themselves may have affected leaflet kinematics because of their weight and bending stiffness of their wires, but to minimize this effect we used small 1-mm leaflet crystals connected to soft wires. Suture annuloplasty is rarely used clinically and whether the similar effect on leaflet mechanics holds true for remodeling rings requires further studies.

CONCLUSIONS

In a chronic ovine model of tachycardia-induced cardiomyopathy with FTR, we found that annular area size reduction of 55% was sufficient to treat FTR but perturbed anterior and PL dynamics while maintaining normal SL motion. More extreme annular reduction triggered profound changes in anterior and PL dynamics, suggesting that very aggressive annular undersizing impairs leaflet kinematics. These data may guide a more physiologic approach to surgical repair of FTR.

Conflict of Interest Statement

Dr Rausch disclosed a speaking agreement with Edwards Lifesciences. All other authors reported no conflicts of interest.

The *Journal* policy requires editors and reviewers to disclose conflicts of interest and to decline handling or reviewing manuscripts for which they may have a conflict of interest. The editors and reviewers of this article have no conflicts of interest.

Dr Malinowski and Dr Jazwiec are the Peter C. and Pat Cook Endowed Research Fellows in Cardiothoracic Surgery.

References

1. Nath J, Foster E, Heidenreich PA. Impact of tricuspid regurgitation on long-term survival. *J Am Coll Cardiol*. 2004;43:405-9.
2. Nishimura RA, Otto CM, Bonow RO, Carabello BA, Erwin JP, Guyton RA, et al. 2014 AHA/ACC guideline for the management of patients with valvular heart disease: a report of the American College of Cardiology/American Heart Association task force on practice guidelines. *J Am Coll Cardiol*. 2014;63:e57-185.
3. McCarthy PM, Bhudia SK, Rajeswaran J, Hoercher KJ, Lytle BW, Cosgrove DM, et al. Tricuspid valve repair: durability and risk factors for failure. *J Thorac Cardiovasc Surg*. 2004;127:674-85.
4. Brescia AA, Ward ST, Watt TMF, Rosenbloom LM, Baker M, Khan S, et al. Outcomes of guideline-directed concomitant annuloplasty for functional tricuspid regurgitation. *Ann Thorac Surg*. 2020;109:1227-32.
5. Huffman LC, Nelson JS, Lehman AN, Krajacic MC, Bolling SF. Identical tricuspid ring sizing in simultaneous functional tricuspid and mitral valve repair: a simple and effective strategy. *J Thorac Cardiovasc Surg*. 2014;147:611-4.
6. Sielicka A, Sarin EL, Shi W, Sulejmani F, Corporan D, Kalra K, et al. Pathological remodeling of mitral valve leaflets from unphysiologic leaflet mechanics after undersized mitral annuloplasty to repair ischemic mitral regurgitation. *J Am Heart Assoc*. 2018;7:1-18.
7. Malinowski M, Jazwiec T, Quay N, Goehler M, Rausch MK, Timek TA. The influence of tricuspid annuloplasty prostheses on ovine annular geometry and kinematics. *J Thorac Cardiovasc Surg*. 2021;161:e191-207.
8. Malinowski M, Jaźwiec T, Goehler M, Bush J, Quay N, Ferguson H, et al. Impact of tricuspid annular size reduction on right ventricular function, geometry and strain. *Eur J Cardiothorac Surg*. 2019;56:400-8.
9. Jazwiec T, Malinowski M, Ferguson H, Wodarek J, Quay N, Bush J, et al. Effect of variable annular reduction on functional tricuspid regurgitation and right ventricular dynamics in an ovine model of tachycardia-induced cardiomyopathy. *J Thorac Cardiovasc Surg*. 2019 [In press].
10. Malinowski M, Proudfoot AG, Langholz D, Eberhart L, Brown M, Schubert H, et al. Large animal model of functional tricuspid regurgitation in pacing induced end-stage heart failure. *Interact Cardiovasc Thorac Surg*. 2017;24:905-10.
11. Malinowski M, Wilton P, Khaghani A, Langholz D, Hooker V, Eberhart L, et al. The effect of pulmonary hypertension on ovine tricuspid annular dynamics. *Eur J Cardiothorac Surg*. 2016;49:40-5.
12. Malinowski M, Jazwiec T, Goehler M, Quay N, Bush J, Jovinge S, et al. Sonomicrometry-derived 3-dimensional geometry of the human tricuspid annulus. *J Thorac Cardiovasc Surg*. 2019;157:1452-61.e1.
13. Rausch MK, Malinowski M, Wilton P, Khaghani A, Timek TA. Engineering analysis of tricuspid annular dynamics in the beating ovine heart. *Ann Biomed Eng*. 2018;46:443-51.
14. Mathur M, Meador WD, Jazwiec T, Malinowski M, Timek TA, Rausch MK. Tricuspid valve annuloplasty alters leaflet mechanics. *Ann Biomed Eng*. 2020; 48:2911-23.
15. Mathur M, Meador WD, Jazwiec T, Malinowski M, Timek TA, Rausch MK. Tricuspid valve leaflet strains in the beating ovine heart. *Biomech Model Mechanobiol*. 2019;18:1351-61.
16. Bolling SF, Deeb GM, Brunsting LA, Bach DS. Early outcome of mitral valve reconstruction in patients with end-stage cardiomyopathy. *J Thorac Cardiovasc Surg*. 1995;109:676-83.
17. Dreyfus GD, Chan KMJ. Functional tricuspid regurgitation: a more complex entity than it appears. *Heart*. 2009;95:868-9.
18. Maghami S, Ghoreishi M, Foster N, Dawood MY, Hobbs GR, Stafford P, et al. Undersized rigid nonplanar annuloplasty: the key to effective and durable repair of functional tricuspid regurgitation. *Ann Thorac Surg*. 2016;102:735-42.
19. Min SY, Song JM, Kim JH, Jang MK, Kim YJ, Song H, et al. Geometric changes after tricuspid annuloplasty and predictors of residual tricuspid regurgitation: a real-time three-dimensional echocardiography study. *Eur Heart J*. 2010;31: 2871-80.
20. Bothe W, Kvitting JPE, Swanson JC, Göktepe S, Vo KN, Ingels NB, et al. How do annuloplasty rings affect mitral leaflet dynamic motion? *Eur J Cardiothorac Surg*. 2010;38:340-9.
21. Tibayan FA, Rodriguez F, Liang D, Daughters GT, Ingels NB, Miller DC. Paneth suture annuloplasty abolishes acute ischemic mitral regurgitation but preserves annular and leaflet dynamics. *Circulation*. 2003;108(Suppl II):128-33.
22. Meador WD, Mathur M, Sugerman GP, Jazwiec T, Malinowski M, Bersi MR, et al. A detailed mechanical and microstructural analysis of ovine tricuspid valve leaflets. *Acta Biomater*. 2020;102:100-13.
23. Kawada N, Naganuma H, Muramatsu K, Ishibashi-Ueda H, Bando K, Hashimoto K. Redefinition of tricuspid valve structures for successful ring annuloplasty. *J Thorac Cardiovasc Surg*. 2018;155:1511-9.e1.
24. Utsunomiya H, Itabashi Y, Mihara H, Kobayashi S, De Robertis MA, Trento A, et al. Usefulness of 3D echocardiographic parameters of tricuspid valve morphology to predict residual tricuspid regurgitation after tricuspid annuloplasty. *Eur Heart J Cardiovasc Imaging*. 2017;18:809-17.
25. Suh YJ, Chang BC, Im DJ, Kim YJ, Hong YJ, Hong GR, et al. Assessment of mitral annuloplasty ring by cardiac computed tomography: correlation with echocardiographic parameters and comparison between two different ring types. *J Thorac Cardiovasc Surg*. 2015;150:1082-90.
26. Matsumiya G, Kohno H, Matsuura K, Sakata T, Tamura Y, Watanabe M, et al. Right ventricular papillary muscle approximation for functional tricuspid regurgitation associated with severe leaflet tethering. *Interact Cardiovasc Thorac Surg*. 2018;26:700-2.
27. Dreyfus GD, Raja SG, Chan KM. Tricuspid leaflet augmentation to address severe tethering in functional tricuspid regurgitation. *Eur J Cardiothorac Surg*. 2008;34:908-10.
28. Kong F, Pham T, Martin C, McKay R, Primiano C, Hashim S, et al. Finite element analysis of tricuspid valve deformation from multi-slice computed tomography images. *Ann Biomed Eng*. 2018;46:1112-27.
29. Bothe W, Rausch MK, Kvitting JPE, Echtner DK, Walther M, Ingels NB, et al. How do annuloplasty rings affect mitral annular strains in the normal beating ovine heart? *Circulation*. 2012;126(11 Suppl 1):S213-38.
30. Laurence D, Ross C, Jett S, Johns C, Echols A, Baumwart R, et al. An investigation of regional variations in the biaxial mechanical properties and stress

relaxation behaviors of porcine atrioventricular heart valve leaflets. *J Biomech*. 2019;83:16-27.
31. Jett S, Laurence D, Kunkel R, Babu AR, Kramer K, Baumwart R, et al. An investigation of the anisotropic mechanical properties and anatomical structure of porcine atrioventricular heart valves. *J Mech Behav Biomed Mater*. 2018;87:155-71.
32. Votta E, Maisano F, Bolling SF, Alfieri O, Montevecchi FM, Redaelli A. The Geoform disease-specific annuloplasty system: a finite element study. *Ann Thorac Surg*. 2007;84:92-101.
33. Krishnamurthy G, Itoh A, Bothe W, Swanson JC, Kuhl E, Karlsson M, et al. Stress-strain behavior of mitral valve leaflets in the beating ovine heart. *J Biomech*. 2009;42:1909-16.
34. Merryman WD, Youn I, Lukoff HD, Krueger PM, Guilak F, Hopkins RA, et al. Correlation between heart valve interstitial cell stiffness and transvalvular pressure: implications for collagen biosynthesis. *Am J Physiol Heart Circ Physiol*. 2006;290:224-31.
35. Pham T, Sulejmani F, Shin E, Wang D, Sun W. Quantification and comparison of the mechanical properties of four human cardiac valves. *Acta Biomater*. 2017;54:345-55.
36. Llaneras MR, Nance ML, Streicher JT, Lima JAC, Savino JS, Bogen DK, et al. Large animal model of ischemic mitral regurgitation. *Ann Thorac Surg*. 1994;57:432-9.
37. Hutchison J, Rea P. A comparative study of the morphology of mammalian chordae tendineae of the mitral and tricuspid valves. *Vet Rec Open*. 2015;2:e000150.
38. Jazwiec T, Malinowski M, Proudfoot AG, Eberhart L, Langholz D, Schubert H, et al. Tricuspid valvular dynamics and 3-dimensional geometry in awake and anesthetized sheep. *J Thorac Cardiovasc Surg*. 2018;156:1503-11.

Key Words: annuloplasty, leaflet strain, tricuspid valve, undersizing

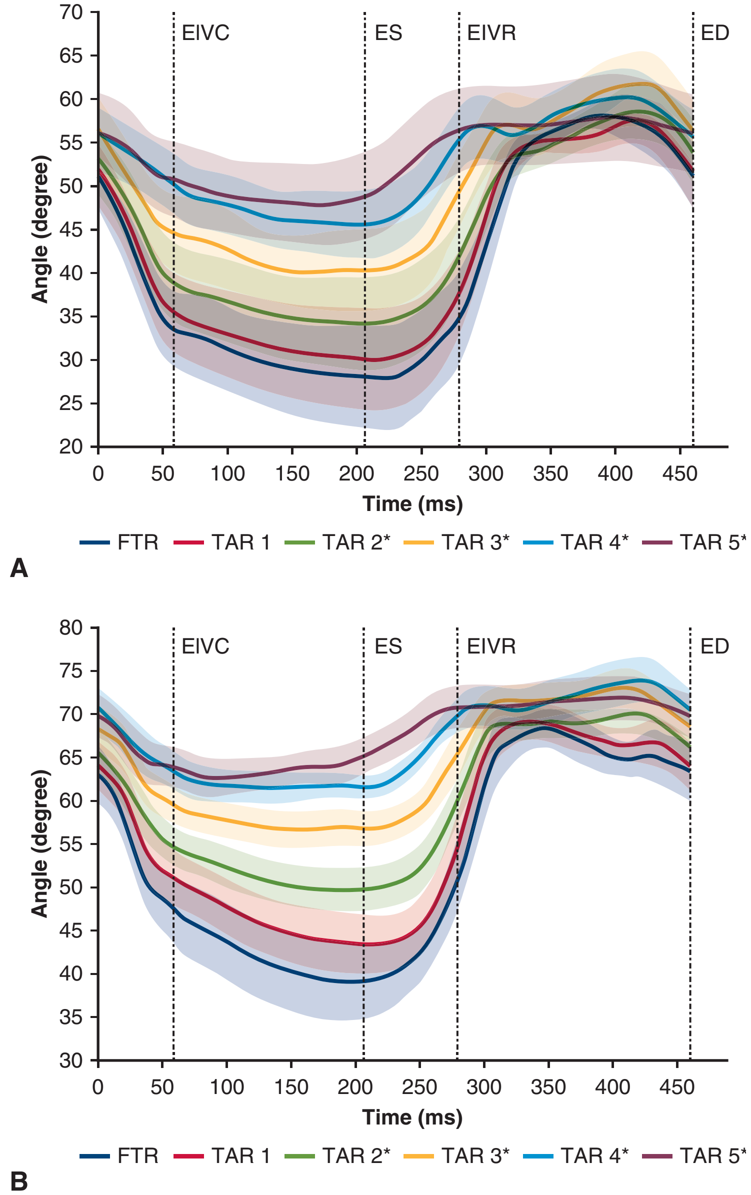

FIGURE E1. Tricuspid leaflet angles during cardiac cycle in FTR and with various degrees of annular size reduction (TAR1-5). A, AL. B, PL. C, SL. *$P < .05$ repeated-measures ANOVA/Friedman ANOVA followed by paired *t* test or Wilcoxon signed-rank test versus FTR at ES. *EIVC*, End of isovolumic contraction; *ES*, end-systole; *EIVR*, end of isovolumic relaxation; *ED*, end-diastole; *FTR*, functional tricuspid regurgitation; *TAR*, tricuspid annular reduction.

BS

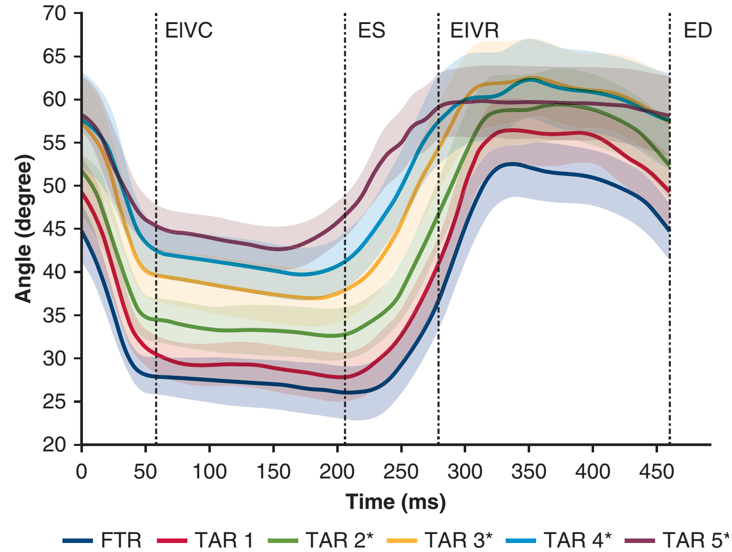

C

FIGURE E1. (*continued*).